Journal of
Materials Chemistry B

Accepted Manuscript

This article can be cited before page numbers have been issued, to do this please use: J. Zhu, J. Zou, J. Zhang, Y. Sun, X. Dong and Q. Zhang, *J. Mater. Chem. B*, 2019, DOI: 10.1039/C9TB00180H.

ROYAL SOCIETY OF CHEMISTRY

rsc.li/materials-b

View Article Online
DOI: 10.1039/C9TB00180H

Journal of Materials Chemistry B

ARTICLE

Anthracene functionalized BODIPY derivative with singlet oxygen storage ability for photothermal and continuous photodynamic synergistic therapy

Received 00th January 2018,
Accepted 00th January 2018

DOI: 10.1039/x0xx00000x
www.rsc.org/

Jianwei Zhu [ab], Jianhua Zou[b], Jie Zhang[a], Yang Sun[a] , Xiaochen Dong[b]*, Qi Zhang[a]*

Singlet oxygen ($^1O_2$) generated from the photosensitized process within tumor tissues during photodynamic therapy (PDT) is self-limiting. Fractional delivery of light tends to be a better method for PDT. Herein, BDPIA with a high $^1O_2$ quantum yield (QY) of 70% in DCM has an additional anthracene module for capturing $^1O_2$, which would be useful in PDT. In the light cycle, the endoperoxide of anthracene is generated with singlet oxygen while in the dark cycle, the endoperoxide undergoes thermal cycloreversion to produce $^1O_2$, regenerating the anthracene module. Therefore, the photodynamic process can continue in the dark period as well as the light cycles, promising their continuous phototherapy efficacy. In addition, BDPIA NPs in water exhibit a high photothermal conversion efficiency (η = 38.9%) for effective photothermal therapy. *In vitro* MTT assay shows that BDPIA NPs have a low half inhibitory concentration (IC_{50}) of 6.293 μg/mL on HeLa cells. Furthermore, lentiviral vectors transfected HeLa cell lines with red fluorescent proteins was used to perform the real time *in vivo* fluorescence imaging guided phototherapy. The model can monitor the real-time uptake of BDPIA NPs. The results indicate that BDPIA NPs are capable of inhibiting cell proliferation even at a low dosage (0.2 mg/kg) while the normal tissues (heart, liver, spleen, lung and kidney) suffer from no side effects. Our results demonstrate that BDPIA NPs with high phototoxicity, low dark toxicity and excellent bio-compatibility can be used a potential photosensitizer for continuous photodynamic and photothermal synergistic therapy.

Introduction

With the increase in the incidence and mortality of cancer in modern society, traditional treatments, including surgery, chemotherapy and radiotherapy, usually have inherent limitations such as resistance, side effects, low targeting and lack of specificity, hence the need for effective and innovative cancer treatments is still urgent.

Over the past decades, photodynamic therapy (known as PDT) has been universally acknowledged as a promising approach to treat various cancers.[1-13] The therapeutic procedure usually involves the photosensitized generation of singlet oxygen ($^1O_2$), and destroys tumor cells and tumor blood vessels. However, PDT itself creates acute hypoxia by rapidly consuming intracellular oxygen reservation, and tumor tissues usually have an inherent hypoxic microenvironment, which resulting in the limit of the photosensitizer's treatment effect.[14] Many studies suggest that intermittent delivery of light might be a better approach to PDT.[6] Since the photothermal effect of the tumor can promote the absorption of deep oxygen in the tumor, the photosensitizer combined with photodynamic therapy and photothermal therapy can overcome the dependence of oxygen to some extent. At the same time, the assistance of photothermal effect is advantage to better transportation and uptake in the tumor for drugs. Thus, the therapeutic effect would be enhanced by

a. School of Pharmaceutical Sciences, Nanjing Tech University (NanjingTech), 30 South Puzhu Road, Nanjing 211800, China. **E-mail: zhangqi@njtech.edu.cn*

b. Key Laboratory of Flexible Electronics (KLOFE) & Institute of Advanced Materials (IAM), Nanjing Tech University (NanjingTech), 30 South Puzhu Road, Nanjing, 211800, China, **E-mail: iamxcdong@njtech.edu.cn*

†Electronic Supplementary Information (ESI) available.

View Article Online
DOI: 10.1039/C9TB00180H

combining photodynamic therapy with photothermal therapy. Considering the fact that singlet oxygen is the cytotoxic agent required for effective PDT, while the characteristics, such as short lifetime and the generation only during the irradiation periods, impeded its effect on tumor cells. [14] Thus, the application of chemically generated singlet oxygen for the dark period is highly desirable for fractional PDT, in which photosensitized generation is impossible. In fact, the combination of a photosensitizer and a chemical source of single molecule would be a wiser approach.[15]

The endoperoxides of anthracene and its derivatives have been acknowledged as reliable chemical sources of singlet oxygen, because they tend to undergo clean cycloreversion reactions without side reactions to release singlet oxygen with very high yields. So far, relevant investigations have been already reported that thermal decomposition of anthracene endoperoxides can produce singlet oxygen, leading to cell death by a process resembling apoptosis. [6, 10-12]

Dipyrromethene, known as BODIPY, are well recognized for their high photostability, and high fluorescence *etc*, which makes them potential candidates for PDT. [16-29] However, their singlet oxygen generation ability is usually disappointingly low. Conjugating heavy atoms can effectively improve the spin obit crossing (SOC) and therefore the singlet oxygen generation quantum yield ($^1O_2$ QY) can be dramatically elevated. Inspired by these observations, one anthracene grafting BODIPY compound, namely, BDPIA (3,7-bis((E)-2-(anthracen-9-yl)vinyl)- 5,5-difluoro-2,8-diiodo- 1,9-dimethyl-10- phenyl-5H-dipyrrolo[1,2-c:2',1'-f][1,3,2]diazaborinin-4-ium-5-uide) has been designed and prepared. The compound has a high $^1O_2$ QY of 70% and the anthracene module can be used for capturing $^1O_2$ to form endoperoxide in the light cycle. While in the dark cycle, the endoperoxide undergoes thermal cycloreversion to produce $^1O_2$, regenerating the anthracene module. The reversible $^1O_2$ storage and delivery can be achieved by changing illumination or not. Also, nanoprecipitation was used to prepare the nanoparticles (NPs) of BDPIA. Similarly, these NPs are able to show reversible $^1O_2$ trapping and releasing ability by using singlet oxygen sensor green (SOSG) as a detecting probe, which promising their potential for continuous PDT therapy. *In vitro* MTT assay indicates that such NPs have a low half inhibitory concentration (IC_{50}) of 0.3715 μg/mL. Furthermore, *in vivo* fluorescence imaging guided phototherapy suggests that BDPIA NPs are capable of inhibiting the growth of tumor under laser irradiation while cause no side effects on normal tissues (heart, kidney, liver, spleen and lung). Our results demonstrate that BDPIA NPs with good bio-compatibility, low dark toxicity, and high phototoxicity are promising for PTT and continuous PDT.

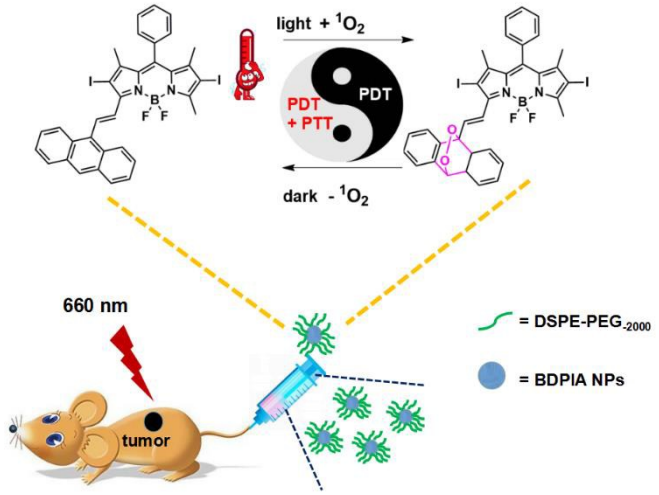

Scheme 1. Illustration of BDPIA NPs for PDT/PTT synergistic therapy and the mechanism of reversible $^1O_2$ capture and delivery.

Experimental

Materials and apparatus

All the chemicals were purchased from Sigma (Shanghai Co.ltd) and used without further purification. The ^{1}H NMR and ^{13}C NMR spectra were measured on Bruker DRX NMR spectrometer (500 MHz) in $CDCl_3$ solution at 298 K as the internal standard with solvent residual ($CDCl_3$, δ = 7.26 ppm). UV-vis spectra were recorded on a spectrophotometer (UV-3600 UV-Vis-NIR, Shimadzu, Japan). The fluorescence spectra were measured on an F-4600 spectrometer (HITACHI, Japan).

Synthesis of BDPIA

A mixture of BDPI (0.575 g, 0.1 mmol), anthracene-9-carbaldehyde (0.412 g, 0.2 mmol) was dissolved in DMF (3 mL), which was heated to 150 °C for 4 h under the catalysis of acetic acid (0.4 mL) and piperidine (0.4 mL). Then the mixture was poured into 150 mL water and extracted with dichloromethane. The organic layer was washed with brine and dried with anhydrous sodium sulfate. The solvent was removed by rotary evaporation, and the crude product was purified by column chromatography (silica gel, DCM:PE = 1:2, v/v). ^{1}H NMR ($CDCl_3$, 400 MHz): δ (ppm) 8.44 (1H, s), 8.39-8.35 (2H, d), 8.27-8.21 (1H, d), 8.05-8.00 (2H, t), 7.56-7.53 (4H, m), 7.52-7.47 (3H, d), 7.35-7.36 (2H, m), 6.92 (1H, s), 260 (3H, s), 1.52 (3H, s), 1.42 (3H, s). ^{13}C NMR (75 MHz, $CDCl_3$): δ (ppm) 137.7, 131.6, 129.3, 128.4, 120.0, 117.5, 113.6, 127.2, 111.2, 44.2, 31.5, 29.9, 29.4, 14.4, 13.9, 12.4. MS: calcd. m/z = 764.02; found m/z = 764.10.

View Article Online
DOI: 10.1039/C9TB00180H

Singlet oxygen detection in DCM and water

Singlet oxygen generation ability was measured by DPBF (1,3-diphenylisobenzofuran) as the $^1O_2$ indicator. The absorbance of DPBF was adjusted around 1.0 while that of BDPIA was around 0.2 to 0.3. After exposing the mixture of BDPIA and DPBF in DCM to laser, the spectra were recorded. To investigate the singlet oxygen generation without laser irradiation, the mixture of BDPIA and DPBF in DCM was irradiated by laser (660 nm, 0.5 W/cm^2), and the absorbance was recorded. The singlet oxygen quantum yield is calculated according to equation (1)

$$\Phi_{\Delta(sam)} = \Phi_{\Delta(std)} \times \frac{S_{sam}}{S_{std}} \times \frac{F_{std}}{F_{sam}} \quad (1)$$

where *sam* and *std* designate the sample and standard substance, respectively. *S* stands for the slope of plot of the absorbance of DPBF (at 418 nm) versus irradiation time, and *F* can be calculated by F= 1-10^{-OD} (OD represents the optical density of sample and MB at 660 nm).

After being stored in the dark for 5 min, the absorbance was recorded again. The singlet oxygen generation ability of BDPIA NPs in water was investigated with SOSG with a probe. The fluorescence was recorded after laser irradiation. The spectrum was recorded again after 5 min. The procedure was repeated for three times.

Preparation of BDPIA nanoparticles

Nanoprecipitation was used to prepare the nanoparticles of BDPIA. DSPE-PEG$_{2000}$ (1 mg) and BDPIA (5 mg) was dissolved in THF (1 mL). Then 200 µL of BDPIA (5 mg/mL) was added into distilled water (5 mL) under vigorous stirring at room temperature. Then the mixture was stirred for 20 min, THF was removed by nitrogen bubbling. BDPIA NPs in the solution were obtained by centrifugation. The photothermal conversion efficiency was calculated according to equation (2).

$$\eta = \frac{hs(T_{max} - T_{amb}) - Q_{Dis}}{I(1 - 10^{-A660})} \quad (2)$$

$$\theta = \frac{T - T_{amb}}{T_{Max} - T_{amb}} \quad dt = -\tau s \frac{d\theta}{\theta} \quad \tau_s = \frac{\sum_i m_i C_{p,i}}{hs} \quad t = -\tau s \ln(\theta)$$

where *h* is the heat transfer coefficient, *S* is the surface area of the container, and the value of *hs* is obtained from the Figure 2d. The T_{max} is the temperature change of BDPIA NPs aqueous solution at the maximum steady-state temperature, I is the laser power, A_{660} is the absorbance of the BDPIA NPs at 660 nm, and Q_{Dis} expresses the heat associated with light absorption by the solvent. The variable τ_s is the sample-system time constant, and m_i and C_i are the mass and heat capacity of the deionized water used as the solvent.

Lentiviral vectors with red fluorescent proteins for transfection of HeLa cell lines

HeLa cell lines (Institute of Biochemistry and Cell Biology, SIBS, CAS (China)) were cultured in a regular growth medium consisting of Dulbecco's modified Eagle's medium (DMEM, Gibco), supplemented with 10% fetal bovine serum under an atmosphere of 5% CO_2 at 37°C. Lentivirus (with red fluorescent proteins, 10^9 TU/mL) was purchased from Genepharma (Shanghai, China). Puromycin Dihydrochloride was obtained from Beyotime Biotechnology (Shanghai, China). Cells were seeded into 24-well plates with 5×10^4/well in 500 µL culture medium. The cells were incubated for 24 h and then exposed to Lentivirus at a series concentration (The values of Multiplicity of Infection were 10, 20, 30, 50, 70, 100). Then the 24-well plate was incubated for another 48 h. Thereafter the previous medium was removed, and added new fresh culture medium containing 5 µg/mL Puromycin Dihydrochloride, the 24-well plate was continuously incubated for another 24 h to remove the cells which were failed to be transfected. The fluorescence images are observed by an Olympus IX 70 inverted microscope to evaluate the transfection efficiency, and the Optimized MOI value was 50. The stable HeLa cell lines with Red fluorescent proteins were established for the following experiments in this study.

MTT assay

Cell viability assay of the nanoparticles was done. First the NPs were dissolved in distilled water and diluted with DMEM to various concentration and put in the 96-well plate, respectively. Then the 96-well plate was irradiated with laser (660 nm, 0.5 W/cm^2) for 5 minutes. Cell viability was determined by colorimetric MTT assay. A solution of 3-(4,5-Dimethylthiazol- 2-yl)-2,5- diphenyltetrazolium bromide (MTT) in distilled water (5 mg/mL, 20 µL) was added to each well, followed by incubation for 3.5 h. Then the medium was discarded and 200 µL DMSO was added at ambient temperature. The optical absorbance was recorded at 492 nm by a Thermo Multiskan Mk3 Microplate Reader. The cell growth inhibitory effects were calculated by the following equation: cell viability (%) = (Atreatment / Acontrol) × 100 %. A cell growth inhibition curve was generated by plotting cell growth inhibition against drug concentration, and the half-maximal inhibitory concentration (IC_{50}) was determined using GraphPad Prism 6 software (GraphPad Software, Inc., La Jolla, CA, USA).

View Article Online
DOI: 10.1039/C9TB00180H

Annexin V-FITC/ propidium iodide (PI) staining

The Apoptosis was analyzed using Annexin V-FITC/propidium iodide (PI) dual staining. HeLa cells were plated in 6-well plates and assigned into three groups (control group, illumination group and without illumination group). After treatment with nanoparticles at concentration of 1 μg/mL, illumination group was irradiated with laser (660 nm, 0.5 W/cm^2) for 5 minutes and incubated for anther 24h, Finally, all the HeLa cells were harvested and stained with Annexin V-FITC/PI Cell Apoptosis Detection Kit (KeyGen Biotech, Nanjing, China) according to the manufacturer's protocol. The apoptosis rates of the cells were then analyzed by a flow cytometer (BD Biosciences, San Jose, CA, USA).

Cellular uptake and fluorescence imaging of cellular ROS

HeLa cells were incubated with BDPIA NPs (6 μg/mL, 2 mL) in a confocal dish for 24 h in dark, the previous medium was discarded, followed by the addition of 1 mL polyoxymethylene for 25 min. Then polyoxymethylene was discarded and the cells were washed with PBS three times. The sample with BDPIA NPs for 24 h was further incubated with 10 μM of 2,7-dichlorodihydrofluorescein diacetate (DCF-DA) for another 3 min, which was washed with 1 mL PBS three times. This sample was irradiated by laser (660 nm, 0.5 W/cm^2) for 1 minutes. The fluorescence images of were observed by Olympus IX 70 inverted microscope. For the cellular uptake samples , they were excited at the wavelength of 633 nm and collected fluorescence from 650 to 750 nm. While the samples for fluorescence imaging of cellular ROS, they were excited with 488 nm laser and collected fluorescence from 490 to 600 nm.

Histology examination and bioimage *in vivo* tumor treatment

The animal ethic approval was obtained from Animal Center of Nanjing Medical University (NJMU, Nanjing, China). 12 nude mice were purchased and then injected with HeLa cells into the armpit as the tumor source. When the tumor volume reached about 80 mm^3, the mice were divided into 3 groups randomly. For the illumination and without illumination group, the mice were intravenously injected with BDPIA NPs (60 μg/mL, 100 μL) in PBS solution, while for the control group, saline was injected. 4 hours after administration, the tumors of the illumination group were irradiated for 8 minutes while the mice in the other two groups were not additionally irradiated. The process above was repeated until the tumor disappears. The tumor volume and body weight of mice were recorded every two days. Finally, these nude mice were sacrificed, followed by the histology analysis. In details, the tumor and major organs (heart, liver, spleen, lung, kidney) from each mouse were isolated and fixed in 4% formaldehyde solution. After dehydration, the tissues were embedded in paraffin cassettes and stained with hematoxylin and eosin (H&E), the images were recorded on a microscope. The bioimages of tumor, heart, liver, spleen, liver and kidney were recorded on PerkinElmer IVIS Lumina K.

Results and Discussion

Synthesis, characterization of BDPIA and its NPs

The synthetic route of BDPIA was proposed in Figure S1 (supporting information), which has been fully structurally characterized by ^{1}HNMR, ^{13}CNMR and mass spectrometry. Generally, reactions of benzoyl chloride with 2,4-dimethylporrole in DCM, followed by the addition of triethylamine and $BF_3{\cdot}OEt_2$ give BDP. Then, BDP was treated with NIS (N-iodosuccinimide) in a mixture of chloroform and acetic acid ($CHCl_3$/HOAc *V/V* 3:1) to produce BDPI. Eventually, BDPIA could be obtained by treating BDPIA and anthracene-9-carbaldehyde through a knoevenagel condensation using acetic and piperidine as catalyst in moderate yield. As shown in Figure 1a, the absorbance of BDPIA in THF shows the maximum intensity at 628 nm while red shift of 55 nm of DSPE-PEG$_{2000}$ coated BDPIA NPs was observed, this can be explained by either the solvent effect or the aggregation of BDPIA.

Singlet oxygen detection with or without irradiation

High singlet oxygen generation ability of photosensitizer is crucial to photodynamic therapy. DPBF was used as the singlet oxygen probe to evaluate the singlet oxygen quantum yield of BDPIA using methylene blue (MB) as the standard substance (Φ_Δ = 57% in DCM). As shown in Figure 2b, 2c, DPBF exhibits a quite high degradation speed under the presence of BDPIA with laser irradiation (660 nm, 0.5 W/cm^2), compared with that of MB in DCM (Figure S2). The singlet oxygen is calculated to be 70%, which can be explained by the so-called heavy atom effect.

Anthracene is an interesting group that can be used as $^1O_2$ detector. The mechanism of this process usually contains the $^1O_2$ addition to the anthracene to form anthracene endoperoxides with light irradiation. While in the dark condition, the $^1O_2$ can be released from the anthracene endoperoxides to form anthracene, which is a reversible process.[6, 12, 14] To investigate the $^1O_2$ storage and release ability of BDPIA in DCM with or without irradiation, the

View Article Online
DOI: 10.1039/C9TB00180H

degradation of DPBF is also reported. As shown in Figure 1d, the absorbance of DPBF decreases with laser irradiation, further degradation was also observed when the solution was stored in dark for another 5 min, showing the continuous $^1O_2$ release ability of such compound. The process was conducted for 4 cycles, obvious degradation could be always detected, indicating the repeatability of such process. Since the $^1O_2$ quantum yield of BDPIA is as high as 70%, it can effectively generate $^1O_2$ with laser irradiation. It is assumed that part of the $^1O_2$ can be captured by the addition reaction with anthracene to form endoperoxides (Scheme 1.). These $^1O_2$ can be released again without irradiation, promising the continuous photodynamic efficacy of such compound.

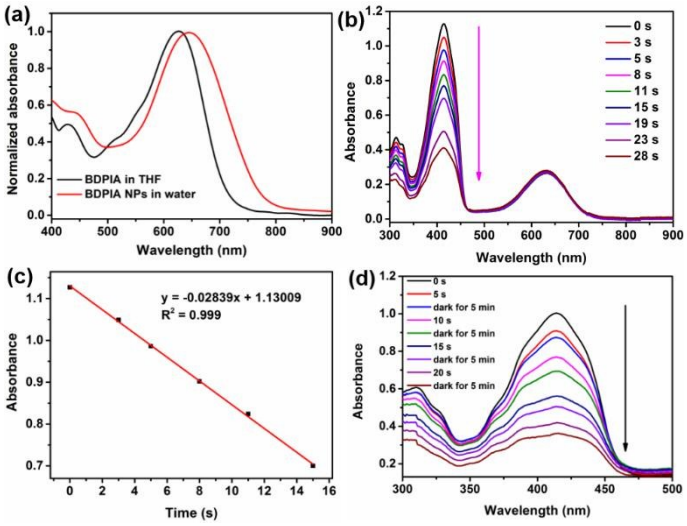

Figure 1 (a) Normalized absorbance of BDPIA in THF and NPs in water. (b) Degradation of DPBF in the presence of BDPIA for different time. (c) Linear fitting of the degradation of DPBF. (d) Degradation of DPBF in the presence or absence of laser irradiation, showing the singlet oxygen generation without irradiation.

Singlet oxygen generation and photothermal conversion efficiency of BDPIA NPs

Nanoprecipitation with DSPE-PEG$_{2000}$ was used to synthesize the NPs to improve the water dispersity of BDPIA. Transmission electron microscope (TEM) and dynamic light scattering (DLS) have been applied to characterize the morphology and size of BDPIA NPs, as shown in Figure 2a. BDPIA can form uniform spherical particles with size distribution from 44 to 285 nm. And the average diameter is 89.3 nm, promising their potential for enhanced penetration and retention (EPR) effect. The TEM result is in good agreement with that of the DLS. To investigate the $^1O_2$ capture and release ability of BDPIA NPs, the fluorescence spectra was recorded using SOSG (singlet oxygen sensor green). Figure 2b shows that the fluorescence intensity of SOSG was greatly enhanced with laser irradiation. When the solution was put in dark for another 5 min, the intensity keeps rising, indicating the $^1O_2$ release from BDPIA NPs. Similarly, the absorbance increases when the process was repeated three times, indicating the continuous $^1O_2$ release, which is consistent with the results of BDPIA in DCM mentioned above.

From the point view of synergistic therapy, combining photodynamic therapy and photothermal therapy is a wise strategy for cancer treatment. When the NPs was prepared, BDPIA will suffer from aggregation caused quenching (ACQ). The NPs with NIR absorbance can convert energy to heat by non-radiative transition upon light irradiation, thus lead to the photothermal ability. To evaluate the photothermal conversion ability of BDPIA NPs, photothermal conversion efficiency was calculated by recording the temperature elevation with irradiation and cooling process without irradiation of BDPIA NPs. As illustrated in Figure 2c, a temperature elevation of 15.4 °C could be observed with low power laser irradiation (660 nm, 0.5 W/cm^2) while water shows a negligible elevation, only 3.2 °C, indicating the excellent photothermal conversion ability of such NPs. Furthermore, the photothermal conversion efficiency (η) was calculated to be 38.9%, which is higher than that of BDPmPh (27.3%) and BDPbiPh (37.9%) but lower than that of BDPtriPh (60.5%)[30]

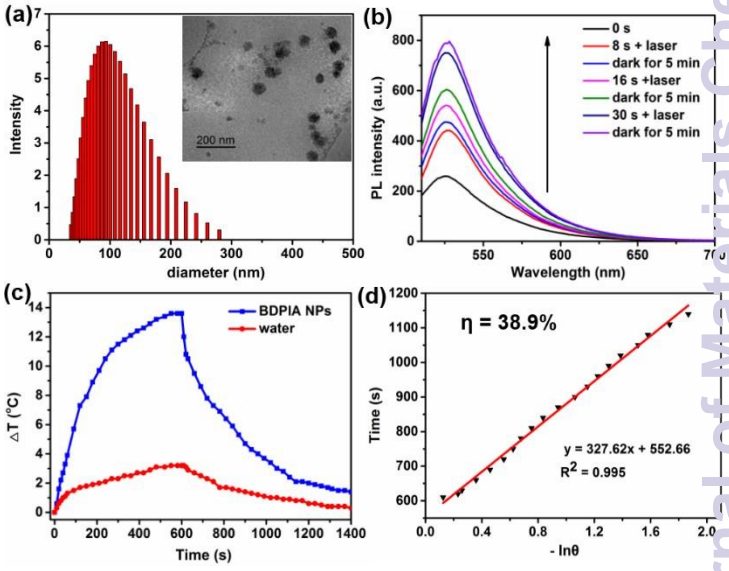

Figure (2) DLS and TEM of BDPIA NPs in water. (b) Fluorescence enhancement of SOSG with or without laser irradiation. (c) Temperature elevation of water and BDPIA NPs with laser irradiation (660 nm, 0.5 W/cm^2). (d) Linear

fitting of -lnθ and time in the cooling curve, showing the calculated photothermal conversion efficiency of 38.9%.

In vitro MTT assay, ROS generation and flow cytometry

To validate the synergistic phototherapeutic effects of BDPIA NPs, we evaluated the inhibitory effect of BDPIA NPs on the cell viability of HeLa cells with red fluorescent proteins (Fig. 3c) at different concentrations. After treatment of BDPIA NPs for 24 h, MTT assay shows that the IC50 (the concentration of drug inhibiting 50 % of cells) value of HeLa cells was 0.3715 μg/mL (Fig. 3b). We tried to evaluate only the photodynamic efficacy of BDPIA NPs. We used a lower power laser irradiation (660 nm, 0.2 W/cm^2) to reduce the amount of generated heat, and the MTT results show that the IC_{50} was 15.73 μg/mL, which is much higher than that obtained under a higher laser density (660 nm, 0.5 W/cm^2) (Figure S3).

And then Annexin V-FITC/PI double staining assay was used to confirm the pro-apoptotic effect of BDPTA NPs. Compared with the control group, the apoptotic rates of HeLa cells in illumination group were significantly increased after treatment with BDPTA NPs (Fig. 3d and 3e), which demonstrated that BDPTA NPs induced typical apoptosis in HeLa cells, while the without illumination group has not significant difference, indicating that the BDPTA NPs have low dark toxicity.

Cellular uptake behavior of BDPIA NPs was studied using a confocal live cell imaging system. The results were shown in Fig. 3a. The high intracellular fluorescence intensity in the cytoplasmic matrix (nuclei dyed with DAPI) can be observed, indicating that the BDPIA NPs can be used for cell imaging and therapy in vitro.

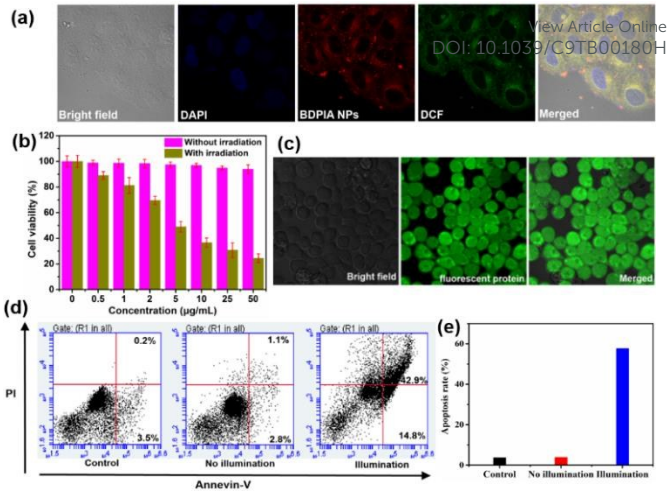

Figure 3 (a) Cellular uptake of BDPIA NPs and ROS generation with DCF-DA as a probe. (b) MTT assay of BDPIA NPs with different conversations. (c) Confocal imaging of HeLa Cells transfected with Lentivirus. (d) Flow cytometry assay (e) Apoptosis rate of control, no illumination and illumination groups.

In vivo fluorescence imaging guided PDT/PTT

The self-fluorescent tumor model was used to investigate the uptake of BDPIA NPs *in vivo*. Double wavelengths (460 and 660 nm) were used as the excitation for different period of time. As illustrated in Figure 4a, the tumor could always be excited at 460 nm which is an appropriate time for the excitation of the red fluorescent proteins. As mentioned in Figure 1a, BDPIA NPs shows strong absorbance around 660 nm, so it was used as the excitation wavelength. For 0 h, no obvious fluorescence can be detected when excited at 660 nm. 2 h after intravenous injection BDPIA NPs, the fluorescence become stronger, indicating the uptake of the BDPIA NPs by enhanced penetration and retention effect (EPR). 4 h after injection, the fluorescence reaches the peak, showing that 4 h is the best time point for phototherapy, and the fluorescence could still be detected 24 h after administration. The mouse was then sacrificed and the fluorescence imaging of tumor, heart, liver, spleen, lung and kidney were recorded. Figure 4b also demonstrates that the fluorescence intensity of the tumor is the highest, followed by liver and kidney, as further confirmed by the quantified intensity of the tissues in Figure 4c. Furthermore, the imaging excited at 460 nm can be well merged with that at 660 nm, this model can accurately display the accumulation process of the BDPIA NPs at the tumor site, showing the advantages and reliability compared with common tumor model.

View Article Online
DOI: 10.1039/C9TB00180H

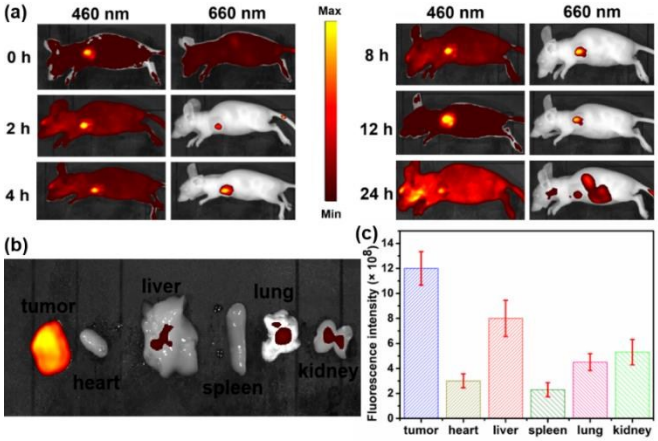

Figure 4 (a) Real-time fluorescence imaging of nude mice under different excitation (460 and 660 nm) for 0, 2 ,4, 8, 12 and 24 h. (b) Fluorescence imaging of tumor, heart, liver, spleen, lung and kidney of the sacrificed nude mice after 24 h injection. (c) Fluorescence intensity of the tumor, heart, liver, lung and kidney.

In vivo photothermal imaging and phototherapy

Owing to the high photothermal conversion efficiency of BDPIA NPs in water, photothermal imaging were recorded to show the temperature elevation to evaluate the photothermal therapy efficacy of BDPIA NPs *in vivo*. As indicated by the fluorescence imaging, post-injection for 4 h is the most suitable time point for phototherapy, 4 h after dosing, the mouse was irradiated at 0, 2, 4, 6, 8 min, respectively. For the control group, the tumor site temperature only increased by 4.2 °C, which was almost negligible. In contrast, when the mouse was injected with BDPIA NPs, the temperature can increase to 51.3°C under the same condition, which is high enough to kill the HeLa cells (Figure 5a, 5b). Due to the excellent phototherapy efficacy of BDPIA NPs, the treatment *in vivo* was performed. In order to evaluate the antitumor effect and toxicity of this BDPIA NPs, the tumor volume and body weight were recorded every two days. As shown in Figure 5c, the tumors in the illumination group disappeared after treatment for 6 days and no recurrence were observed when the mice were kept for another 10 days, demonstrating the complete ablation of the tumor. While in the control group and without illumination group, the eventual relative tumor volume are 12.1 and 11.8 times bigger than that of the original one, respectively, and there was no significant difference between the two groups, showing the low dark toxicity of BDPIA NPs. The mice after treatment were shown in Figure S4.

Furthermore, compared with control group, the body weight changes of the other two groups can also suggest that the BDPIA NPs have no side effects because the weight tend to increase during the therapy process.

After treatment, these nude mice of the three groups were sacrificed and photographs of the tumors were illustrated in Figure 5e. Then the H&E stained pictures of the tumors in the control and no illumination groups were shown in Figure 5f and 5g, the nucleus of HeLa cells remain common and no obvious distortion was observed, suggesting the low dark toxicity of BDPIA NPs. Furthermore, the H&E stained pictures of the normal tissues indicate that such NPs cause no damage to heart, liver, spleen, lung and kidney, showing the low dark toxicity and good bio-compatibility (Figure 6). [31-37] In conclusion, BDPIA NPs with high phototoxicity, excellent bio-compatibility and low dark toxicity would be a potential candidate drug for anti-cancer treatment.

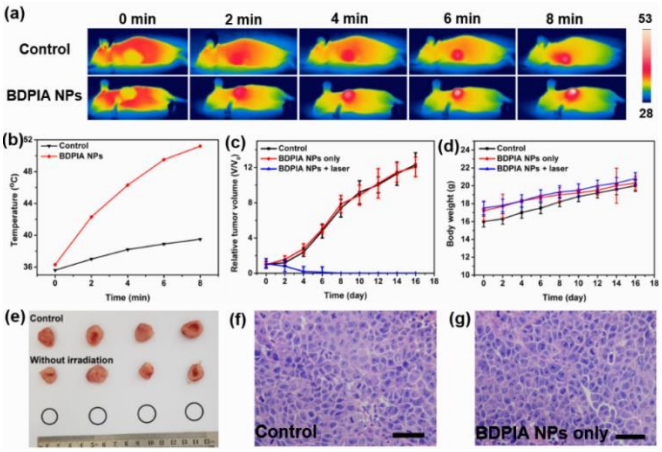

Figure 5 (a) *In vivo* photothermal imaging of the nude mice after injection with PBS or BDPIA NPs under laser irradiation. (b) Temperature elevation of the group injected with PBS or BDPIA NPs under laser irradiation (660 nm, 0.5 W/cm^2). (c) Relative tumor volume (d) Body weight change of the control, no illumination and illumination groups. (e) Digital photograph of the tumors. H&E stained pictures of (f) control and (g) BDPIA NPs only groups. Scale bar:100 μm.

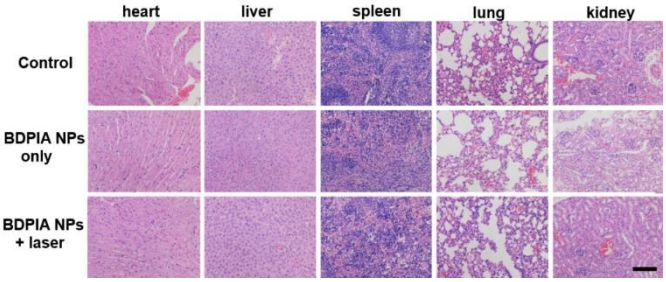

Figure 6 (a) H&E stained picture of heart, liver, spleen, lung and kidney in the control, BDPIA NPs only and BDPIA NPs + laser groups. Scale bar:100 μm.

Conclusions

In conclusion, BDPIA with high $^1O_2$ QY can capture singlet oxygen by the addition reaction with anthracene to form endoperoxides upon laser irradiation. In the dark condition, the singlet oxygen can continuously release without irradiation, which is indicated by the DPBF degradation, meanwhile, BDPIA NPs with good water dispersity can also keep this characteristic, which is proved by SOSG as a probe. Reversible $^1O_2$ storage and release characteristics of BDPIA NPs make them potential candidates for continuous photodynamic therapy. Furthermore, superior phototherapy efficacy can be obtained due to the high photothermal conversion efficiency (38.9%) of BDPIA NPs. Such NPs can effectively inhibit the growth of tumors and cause no adverse effects on normal organs at a low dosage (0.2 mg/kg). The results demonstrate that the continuous photodynamic therapy characteristic can be achieved by appropriate molecular design, and the BDPIA NPs with high phototoxicity, excellent bio-compatibility and low dark toxicity achieve good therapeutic efficiency without obvious side effects, which make them has a great potential for photodynamic and photothermal synergistic therapy.

Acknowledgements

This work was supported by the National Natural Science Foundation of China (No. 81373478), the Natural Science Foundation of Jiangsu Province (No. BK20171024), Key University Science Research Project of Jiangsu Province (15KJA430006), QingLan Project and Program for Innovative Research Team in University of Jiangsu Province.

Conflict of interest

The authors have no conflict of interest to declare.

Notes and references

View Article Online
DOI: 10.1039/C9TB00180H

1. Z. Zhou, J. Song, L. Nie and X. Chen, *Chem Soc Rev*, 2016, **45**, 6597-6626.

2. B. Bertrand, K. Passador, C. Goze, F. Denat, E. Bodio and M. Salmain, *Coord Chem Rev*, 2018, **358**, 108-124.

3. A. Bhattacharyya, A. Jameei, A. Garai, R. Saha, A. A. Karande and A. R. Chakravarty, *Dalton Trans*, 2018, **47**, 5019-5030.

4. H. He, S. Ji, Y. He, A. Zhu, Y. Zou, Y. Deng, H. Ke, H. Yang, Y. Zhao, Z. Guo and H. Chen, *Adv Mater*, 2017, **29**.

5. L. Huang, Z. Li, Y. Zhao, J. Yang, Y. Yang, A. I. Pendharkar, Y. Zhang, S. Kelmar, L. Chen, W. Wu, J. Zhao and G. Han, *Adv Mater*, 2017, **29**.

6. S. Kim, Y. Zhou, N. Tohnai, H. Nakatsuji, M. Matsusaki, M. Fujitsuka, M. Miyata and T. Majima, *Chemistry*, 2018, **24**, 636-645.

7. H. Xiong, H. Zuo, Y. Yan, G. Occhialini, K. Zhou, Y. Wan and D. J. Siegwart, *Adv Mater*, 2017, **29**.

8. Y. Liu, N. Song, L. Chen and Z.G. Xie, *Chinese Journal of Polymer Science*, 2017, **36**, 417-424.

9. J. Zhao, K. Chen, Y. Hou, Y. Che, L. Liu and D. Jia, *Org Biomol Chem*, 2018, **16**, 3692-3701.

10. Z. Yuan, S. Yu, F. Cao, Z. Mao, C. Gao and J. Ling, *Polymer Chemistry*, 2018, **9**, 2124-2133.

11. Z. Wang and J. Zhao, *Org Lett*, 2017, **19**, 4492-4495.

12. M. A. Filatov, S. Karuthedath, P. M. Polestshuk, H. Savoie, K. J. Flanagan, C. Sy, E. Sitte, M. Telitchko, F. Laquai, R. W. Boyle and M. O. Senge, *J Am Chem Soc*, 2017, **139**, 6282-6285.

13. S. Kolemen, Y. Cakmak, Z. Kostereli and E. U. Akkaya, *Org Lett*, 2014, **16**, 660-663.

14. X. Li, N. Kwon, T. Guo, Z. Liu and J. Yoon, *Angew Chem Int Ed Engl*, 2018, DOI: 10.1002/anie.201805138.

View Article Online
DOI: 10.1039/C9TB00180H

15. I. S. Turan, D. Yildiz, A. Turksoy, G. Gunaydin and E. U. Akkaya, *Angew Chem Int Ed Engl*, 2016, **55**, 2875-2878.

16. V. Ramu, S. Gautam, A. Garai, P. Kondaiah and A. R. Chakravarty, *Inorg Chem*, 2018, **57**, 1717-1726.

17. P. Verwilst, H. R. Kim, J. Seo, N. W. Sohn, S. Y. Cha, Y. Kim, S. Maeng, J. W. Shin, J. H. Kwak, C. Kang and J. S. Kim, *J Am Chem Soc*, 2017, **139**, 13393-13403.

18. E. Palao, T. Slanina, L. Muchova, T. Solomek, L. Vitek and P. Klan, *J Am Chem Soc*, 2016, **138**, 126-133.

19. L. Huang, Z. Li, Y. Zhao, Y. Zhang, S. Wu, J. Zhao and G. Han, *J Am Chem Soc*, 2016, **138**, 14586-14591.

20. A. M. Durantini, L. E. Greene, R. Lincoln, S. R. Martinez and G. Cosa, *J Am Chem Soc*, 2016, **138**, 1215-1225.

21. T. Wang, Y. Hou, Y. Chen, K. Li, X. Cheng, Q. Zhou and X. Wang, *Dalton Trans*, 2015, **44**, 12726-12734.

22. L. B. Meng, W. Zhang, D. Li, Y. Li, X. Y. Hu, L. Wang and G. Li, *Chem Commun (Camb)*, 2015, **51**, 14381-14384.

23. S. Guo, L. Xu, K. Xu, J. Zhao, B. Kucukoz, A. Karatay, H. G. Yaglioglu, M. Hayvali and A. Elmali, *Chem Sci*, 2015, **6**, 3724-3737.

24. J. Xu, S. Sun, Q. Li, Y. Yue, Y. Li and S. Shao, *Anal Chim Acta*, 2014, **849**, 36-42.

25. M. Isik, R. Guliyev, S. Kolemen, Y. Altay, B. Senturk, T. Tekinay and E. U. Akkaya, *Org Lett*, 2014, **16**, 3260-3263.

26. A. Barba-Bon, A. M. Costero, S. Gil, A. Harriman and F. Sancenon, *Chemistry*, 2014, **20**, 6339-6347.

27. X. Zhang, Y. Xiao, J. Qi, J. Qu, B. Kim, X. Yue and K. D. Belfield, *J Org Chem*, 2013, **78**, 9153-9160.

28. A. Kamkaew, S. H. Lim, H. B. Lee, L. V. Kiew, L. Y. Chung and K. Burgess, *Chem Soc Rev*, 2013, **42**, 77-88.

29. N. Boens, V. Leen and W. Dehaen, *Chem Soc Rev*, 2012, **41**, 1130-1172.

30. J. Zou, P. Wang, Y. Wang, G. Liu, Y. Zhang, Q. Zhang, J. Shao, W. Si, W. Huang and X. Dong, *Chem Sci*, 2019, **10**, 268-276.

31. J. Zou, Z. Yin, K. Ding, Q. Tang, J. Li, W. Si, J. Shao, Q. Zhang, W. Huang and X. Dong, *ACS Appl Mater Interfaces*, 2017, **9**, 32475-32481.

32. G. Liu, J. Zou, Q. Tang, X. Yang, Y. Zhang, Q. Zhang, W. Huang, P. Chen, J. Shao and X. Dong, *ACS Appl Mater Interfaces*, 2017, **9**, 40077-40086.

33. J. Zou, Z. Yin, P. Wang, D. Chen, J. Shao, Q. Zhang, L. Sun, W. Huang and X. Dong, *Chem Sci*, 2018, **9**, 2188-2194.

34 Z. Yang, R. Tian, J. Wu, Q. Fan, B. Yung, G. Niu, O. Jacobson, Z. Wang, G. Liu, G. Yu, W. Huang, J. Song, X. Chen, *ACS Nano*, **2017**, *11*, 4247-4255.

35 Z. Yang, Y. Dai, C. Yin, Q. Fan, W. Zhang, J. Song, G. Yu, W. Tang, W. Fan, B. Yung, J. Li, X. Li, Y. Tang, W. Huang, J. Song, X. Chen, *Adv. Mater.*, **2018**, *30*, 1707509.

36 Z. Yang, J. Song, W. Tang, W. Fan, Y. Dai, Z. Shen, L. Lin, S. Cheng, Y. Liu, G. Niu, P. Rong, W. Wang, X. Chen, *Theranostics*, **2019**, *9*, 526.

37 Z. Yang, Y. Dai, L. Shan, Z. Shen, Z. Wang, B. Yung, O. Jacobson, Y. Liu, W. Tang, S. Wang, L. Lin, G. Niu, P. Huang, X. Chen, *Nanoscale Horiz.*, **2019**, *4*, 426-433